Topological susceptibility on the lattice: The two-dimensional O(3) σ model

Adriano Di Giacomo
Dipartimento di Fisica dell'Università and Istituto Nazionale di Fisica Nucleare, Piazza Torricelli 2, I-56100 Pisa, Italy and CERN, Theory Division, CH-1211 Geneva 23, Switzerland

Federico Farchioni, Alessandro Papa, and Ettore Vicari
Dipartimento di Fisica dell'Università and Istituto Nazionale di Fiscia Nucleare, Piazza Torricelli 2, I-56100 Pisa, Italy
(Received 11 March 1992)

As a test of the procedures used in lattice gauge theories, we study the topological susceptibility χ in a two-dimensional O(3) σ or CP^1 model. We determine χ by defining the density of topological charge as a local operator on the lattice. Following the prescriptions of field theory we perform the additive and multiplicative renormalizations needed to extract χ from Monte Carlo data. We also determine χ by the cooling method, finding consistent results. A combined use of cooling and field theory again gives the same result and insight into the renormalization mechanism. Finally we give a direct determination, by Monte Carlo techniques, of both the multiplicative and additive renormalizations, by heating configurations with a definite number of instantons. The results are consistent with perturbation theory.

PACS number(s): 11.15.Ha, 12.38.Gc, 75.10.Jm

I. INTRODUCTION

Topology plays an important role in quantum chromodynamics. The existence of a nonzero topological susceptibility of the QCD vacuum can solve the so-called U(1) problem [1–3], i.e., the breaking of the U(1) axial symmetry. Chiral Ward identities, combined with a $1/N_c$ expansion, lead to the relation [3]

$$\frac{2N_f}{f_\pi^2}\chi = m_{\eta'}^2 + m_\eta^2 - 2m_k^2 \ . \tag{1}$$

With $N_f=3$ light flavors, the value of χ required by Eq. (1) to explain the observed value of $m_{\eta'}$ is

$$\chi \simeq (180 \text{ MeV})^4 \ . \tag{2}$$

Equation (1) being derived from an expansion $1/N_c$, the topological susceptibility is intended to be that of a pure gauge system, with no quarks [3,2].

A determination of χ is out of the reach of perturbation theory. Simulation of the theory on the lattice is the only known tool to compute it. Indeed, as will be discussed in what follows, lattice determinations of χ in QCD do exist, and are consistent with the value given in Eq. (2). However, extracting topology from the discrete configurations of the lattice proves to be a nontrivial task. The origin of the difficulties is that lattice simulations produce a regularized version of the theory, with lattice spacing a as a cutoff. Physical quantities such as χ can only be obtained after renormalization, i.e., after removing cutoff-dependent lattice artifacts. Different methods have been developed to do this. The aim of the present paper is to discuss this problem and to test its possible solutions on a simple model, the two-dimensional (2D) O(3) σ model, or CP^1 model. As QCD, this is asymptotically free, it presents dimensional transmutation and has a nontrivial topology. A short presentation of the main results of this paper is already contained in Refs. [4] and [5].

The topological susceptibility χ, in two-dimensional CP^{N-1} models and in four-dimensional non-Abelian gauge theories, is a renormalization-group-invariant quantity, which measures the amount of topological excitations in the vacuum; χ is defined as the correlation at zero momentum of two topological charge-density operators $Q(x)$:

$$\chi = \int d^d x \langle 0|TQ(x)Q(0)|0\rangle \ ; \tag{3}$$

$Q(x)$ is the divergence of a topological current K_μ [1,6], $Q(x)=\partial_\mu K_\mu$. The prescription defining the product of operators in Eq. (3) is [7]

$$\langle 0|TQ(x)Q(0)|0\rangle \equiv \partial_\mu \langle 0|TK_\mu(x)Q(0)|0\rangle \ . \tag{4}$$

This prescription eliminates the contribution of possible contact terms (i.e., proportional to the δ function or its derivatives) when $x \to 0$.

On the lattice, a topological charge-density operator can be defined as having the appropriate classical continuum limit [8]:

$$Q^L(x) \underset{a\to 0}{\sim} a^d Q(x) + O(a^{d+2}) \ , \tag{5}$$

where a is the lattice spacing and d the space-time dimension. In order to determine χ, the correlation at zero momentum of two $Q^L(x)$ operators χ^L is calculated:

$$\chi^L = \left\langle \sum_x Q^L(x)Q^L(0) \right\rangle = \frac{1}{V}\left\langle \left[\sum_x Q^L(x)\right]^2 \right\rangle \ ; \tag{6}$$

χ^L is connected to χ by a nontrivial relation. The presence of irrelevant operators of higher dimension in $Q^L(x)$ induces quantum corrections. Equation (5) must be corrected by including a renormalization constant $Z(\beta)$ [9]:

$$Q^L(x) \underset{a\to 0}{\sim} a^d Z(\beta) Q(x) + O(a^{d+2}) . \tag{7}$$

For SU(N) gauge theories, $\beta = 2N/g_0^2$, with g_0 the coupling constant, for the 2D O(3) σ model $\beta = 1/T$, where T is the temperature; $Z(\beta)$ is a finite function of β, which will tend to 1 when the continuum limit ($\beta \to \infty$) is approached. If a perturbative expansion makes sense, then

$$Z(\beta) = 1 + \frac{z_1}{\beta} + \frac{z_2}{\beta^2} + \cdots . \tag{8}$$

Furthermore, there are contributions of contact terms originating when $x \to 0$ in Eq. (6). A prescription equivalent to Eq. (4) does not exist on the lattice, and therefore the contribution of the contact terms must be isolated and subtracted. These contact terms appear as mixings with the action density $S(x)$ and with the unity operator I, which are the only available operators with equal dimensions or lower. In equation form,

$$\chi^L(\beta) = a^d Z(\beta)^2 \chi + a^d A(\beta) \langle S(x) \rangle + P(\beta) \langle I \rangle + O(a^{d+2}) . \tag{9}$$

The lattice spacing a follows the renormalization-group prediction. For QCD at sufficiently large β,

$$a\Lambda_L = f(\beta) , \qquad f(\beta) \simeq \left[\frac{\beta}{2Nb_0} \right]^{-b_1/2b_0^2} \exp\left[-\frac{\beta}{4Nb_0} \right] , \tag{10}$$

where Λ_L is a mass parameter, b_0 and b_1 are the first coefficients of the renormalization β function. A similar formula gives a as a function of temperature in the 2D O(3) σ model [see Eq. (16)]. Terms of a higher dimension $O(a^{d+2})$ can be neglected at large enough β. The functions $Z(\beta)$, $P(\beta)$, and $A(\beta)$ are renormalization effects and have their origin in the ultraviolet cutoff-dependent modes. Extracting χ from Eq. (9) is not easy: one has to take good care to evaluate these renormalizations, which mask the physical signal. The subtraction of the perturbative tail $P(\beta)$ is the most delicate point, its contribution becoming dominant when $\beta \to \infty$ (it is a series in β^{-1}), since the physical signal falls off exponentially at large β, being a power of a. The hope is that a scaling window exists, i.e., a range of values where β is large enough, for $f(\beta)$ to have already the asymptotic form of Eq. (10), for $Z(\beta)$, $A(\beta)$, and $P(\beta)$ to be well approximated by a few terms of their asymptotic expansion within the statistical errors; but at the same time, β is small enough for the physical signal in Eq. (9), proportional to a^d, to be still detectable with respect to the errors. As we shall see, this proves to be possible in the O(3) σ model, as it is in QCD. Equation (9) is a direct consequence of field theory: if the lattice reproduces field theory in the continuum limit, Eq. (9) must be true.

To overcome the difficulties encountered in extracting χ from Eq. (9), two alternative methods were developed to compute χ. The first one is known as cooling [10]: it consists of measuring the topological susceptibility on an ensemble of configurations cooled by minimizing the action locally. Local changes should not modify the topological properties of a configuration, and its topological content may be extracted from the cooled configuration, where the short-ranged fluctuations, responsible for the renormalization effects, have been eliminated, leading to integer values of $Q = \sum_x Q^L(x)$. A delicate point in cooling is checking for eventual losses of topological charge; such losses would not occur in the continuum, given the global stability of the topological charge. On the lattice, where instantons are only metastable, this charge is bound to vanish eventually, after protracted cooling. The consistency of the field-theoretical and cooling methods was demonstrated for 4D SU(2) [11] and SU(3) [12] gauge theories, and as a by-product a method to control the possible losses of topological charge during cooling was provided.

A third method, the so-called geometrical method [13–17], uses an interpolation among discrete lattice variables to assign an integer topological charge to each lattice configuration. A difficulty associated with this method is that such an assignment is unambiguous only for configurations respecting a certain bound [15], thus excluding many of the configurations actually generated in a numerical simulation. A test of this method on the 2D O(3) σ model [13] gave negative results in that Monte Carlo data did not show the expected scaling behavior, therefore rendering impossible the determination of χ. This failure was explained by the presence of exceptional configurations called dislocations, i.e., topological structures of the size of one lattice spacing, whose unphysical contribution to χ does not vanish in the continuum limit [18]. The geometrical method meets similar difficulties in 4D non-Abelian gauge theories [19]. In order to use this method, one should master the dislocations: a judicious choice of the action, within the same class of universality, might meet the purpose, by reducing the weight of such configurations.

The situation for QCD (for a review, see Ref. [20]) is now that the field-theoretical method and the cooling method give a consistent determination of χ, which is also consistent with the phenomenological estimate (2). A test of the above methods on a theory simpler than QCD, but with some of the same relevant properties, is therefore important.

In this paper we perform this test on the 2D O(3) σ model, or CP^1 model. We determine the topological susceptibility with both the field-theoretical and cooling methods. We find consistency between the two determinations. In addition, we estimate directly by Monte Carlo techniques the renormalizations in Eq. (9). To this purpose the distinction between the fluctuations at a distance $l \sim a$, contributing to the renormalizations, and those at $l \sim \xi$ (ξ being the correlation length), determining the relevant topological properties, is essential. We compare the direct measure of $Z(\beta)$ and $P(\beta)$ with their perturbative estimates, checking the assumption, which already proved to work in QCD, that the perturbative expansion is an asymptotic expansion and that nonperturbative effects do not influence the first few terms of it.

Work is in progress also on CP^{N-1} models with large N; on the one hand, there exist in the literature [18,21] estimates of χ based on an $1/N$ expansion to which the lat-

tice results can be compared; on the other hand, dislocations are expected to be less effective [22] and therefore the χ defined by the geometrical method may have the right continuum limit.

II. RENORMALIZATION AND TOPOLOGICAL SUSCEPTIBILITY

A. The model

The 2D O(3) nonlinear σ model, or CP^1 model, has been widely studied in the literature because it presents similarities with 4D non-Abelian gauge theories. The model is asymptotically free and becomes nonperturbative in the infrared region with spontaneous mass generation. Another important point of contact is the nontrivial topology. As in QCD, nonperturbative effects can be studied by formulating the theory on the lattice and performing Monte Carlo simulations.

The action of the 2D O(3) σ model is

$$S=\frac{1}{2T}\int d^2x[\partial_\mu\phi(x)]^2 , \tag{11}$$

where $\phi(x)$ is a three-component real field satisfying the constraint $\phi\cdot\phi=1$, and T is a coupling which plays the role of a temperature. The topological charge of a spin field $\phi(x)$ is defined by

$$\begin{aligned} Q&=\int d^2x Q(x) , \\ Q(x)&=\frac{1}{8\pi}\epsilon_{\mu\nu}\epsilon_{ijk}\phi_i(x)\partial_\mu\phi_j(x)\partial_\nu\phi_k(x) ; \end{aligned} \tag{12}$$

Q is the number of times $\phi(x)$ winds around the sphere S^2.

We regularize the theory on the lattice by taking the Symanzik tree-level-improved action [23], which offers notable advantages from the point of view of Monte Carlo simulations:

$$S^L=-\beta\sum_{x,\mu}\left[\tfrac{4}{3}\phi(x)\phi(x+\mu)-\tfrac{1}{12}\phi(x)\phi(x+2\mu)\right] , \tag{13}$$

where $\beta=1/T$.

For both continuum and lattice, at low temperature, the perturbative expansion is obtained by setting $\phi\equiv[\pi_i,(1-\sum_i\pi_i^2)^{1/2}]$, $i=1,2$. The quantization of the action introduces an additional ill-defined (infinite) determinant, which is necessary for geometrical reasons: it allows us to write the functional measure over the field π in an O(3)-invariant way. The partition function is

$$\begin{aligned} Z&=\int\prod_x[d\phi(x)\delta(\phi^2(x)-1)]\exp[-S^L(\phi)] \\ &=\int\prod_x\left[d\pi_1(x)d\pi_2(x)\left[1-\sum_i\pi_i^2(x)\right]^{-1/2}\right]\exp[-S^L(\pi)] \\ &=\int\prod_x[d\pi_1(x)d\pi_2(x)]\exp\left\{-\left[S^L(\pi)+\tfrac{1}{2}\sum_x\ln\left[1-\sum_i\pi_i^2(x)\right]\right]\right\} . \end{aligned} \tag{14}$$

In dimensional regularization, the measure term does not contribute, as a consequence of the rule $\int d^dk=0\Longleftrightarrow\delta^d(0)=0$, where d is the space dimension.

The perturbation expansion suffers from infrared divergences, which can be cured by adding a magnetic term to the action:

$$S_M=-\int d^2x\, h\left[1-\sum_i\pi_i^2\right]^{1/2} . \tag{15}$$

Indeed, S_M explicitly breaks the O(3) invariance and acts as a mass term for the π fields. The O(3)-invariant quantities (and the relations among them) are free of infrared divergences, and have a well-defined limit for $h\to 0$.

The lattice spacing a is given by the renormalization-group formula

$$\begin{aligned} a&=\frac{1}{\Lambda_{SY}}f(\beta) , \\ f(\beta)&=2\pi\beta e^{-2\pi\beta}\left[1+\frac{\delta_{SY}}{2\pi\beta}+O(1/\beta^2)\right] , \end{aligned} \tag{16}$$

where δ_{SY} is a numerical constant coming from a three-loop calculation [24]: $\delta_{SY}=0.34$.

A regularized version of $Q(x)$ on the lattice can be obtained by discretizing the derivatives in Eq. (12):

$$\begin{aligned} Q^L(x)=&\frac{1}{32\pi}\epsilon_{\mu\nu}\epsilon_{ijk}\phi_i(x)[\phi_j(x+\mu)-\phi_j(x-\mu)] \\ &\times[\phi_k(x+\nu)-\phi_k(x-\nu)] , \end{aligned} \tag{17}$$

where we have taken a symmetrized version of $\partial_\mu=[\phi(x+\mu)-\phi(x-\mu)]/2a$. In order to extract the topological susceptibility, we calculate the correlation χ^L at zero momentum of two $Q^L(x)$ operators, Eq. (6); χ^L is connected to χ by a nontrivial relation containing the multiplicative renormalization of $Q^L(x)$ and contributions of contact terms originating when $x\to 0$, Eq. (9).

B. Topological charge-density renormalization

On the continuum, $Q(x)$ is invariant under the renormalization group if a suitable renormalization scheme is chosen, for example, the modified minimal subtraction ($\overline{\text{MS}}$) scheme. This can be directly checked by calculating the renormalized two-point proper function of the π field with one insertion of $Q(x)$, $\Gamma^{\overline{\text{MS}}}_{Q\pi\pi}$. Since we are only interested in the renormalization of $Q(x)$, in our calculations we put $p+q=0$ after having factorized the tree-order two-point function $\Gamma^{\text{tree}}_{Q\pi\pi}=-(1/4\pi)\delta_{ij}\epsilon_{\mu\nu}p_\mu q_\nu$ (p and q are the external momenta). We define $F_{Q\pi\pi}$ by the relation $\Gamma_{Q\pi\pi}=\Gamma^{\text{tree}}_{Q\pi\pi}F_{Q\pi\pi}$ and we compute $F_{Q\pi\pi}$ at $p+q=0$. By a calculation at two loops we found (the

corresponding diagrams are shown in Figs. 1 and 2)

$$F^{\overline{\rm MS}}_{Q\pi\pi}(t_r,h_r,\mu;p,q)|_{p+q=0} = Z_\pi(T,\varepsilon)F^B_{Q\pi\pi}(T,h,\varepsilon;p,q)|_{p+q=0} = 1-\frac{2}{4\pi}\ln\frac{h_r}{\mu^2}t_r+\frac{3}{16\pi^2}\ln^2\frac{h_r}{\mu^2}t_r^2+O(t_r^3)\ , \quad (18)$$

where $T=t_r\mu^{-\varepsilon}Z_t$, $h=h_rZ_tZ_\pi^{-1/2}$; here $F^{\overline{\rm MS}}$ and F^B are, respectively, the renormalized and the bare functions; $\varepsilon=d-2$; Z_π is the renormalization constant of the fields π [25]:

$$Z_\pi=1+\frac{1}{\pi\varepsilon}T+\frac{1}{4\pi^2\varepsilon^2}T^2+O(T^3)\ ; \quad (19)$$

$t_r=T\mu^\varepsilon Z_t^{-1}$ is the renormalized coupling, with Z_t given by [25]

$$Z_t=1+\frac{1}{2\pi\varepsilon}T+\left[\frac{1}{4\pi^2\varepsilon^2}+\frac{1}{4\pi\varepsilon}\right]T^2+O(T^3)\ , \quad (20)$$

$h_r=hZ_\pi^{1/2}Z_t^{-1}$ is the renormalized external field; μ is an energy scale. Since the right-hand side (RHS) of Eq. (18) is finite when written in terms of renormalized quantities, it follows that $Q(x)$ does not renormalize up to two loops.

A finite multiplicative renormalization connects the matrix elements of $Q^L(x)$ with those of $Q(x)$, defined in the $\overline{\rm MS}$ scheme. The antisymmetry of $Q^L(x)$ forbids mixings with any other O(3)-invariant operators of dimension 2. We write

$$Q^L(x)=Z(T)Q(x)\ . \quad (21)$$

Since the anomalous dimension of $Q(x)$, $\gamma_Q(t_r)$, is zero, $Z(T)$ must satisfy the equation

$$\gamma_Q(t_r)=\mu\frac{d}{d\mu}\ln Z(T)\bigg|_{T,a}=0\ , \quad (22)$$

and therefore be a finite function of T, which can be determined by imposing [26]

$$F^{\overline{\rm MS}}_{Q\pi\pi}(t_r,h_r,\mu;p,q)=Z^{-1}(T)Z^{\overline{\rm MS}}_\pi(T,\mu,a)\times F^L_{Q\pi\pi}(T,h,a;p,q)\ , \quad (23)$$

with $T=t_rZ_t^{\overline{\rm MS}}$, and $h=h_rZ_t^{\overline{\rm MS}}Z_\pi^{\overline{\rm MS}-1/2}$; $F^L_{Q\pi\pi}$ is defined by $\Gamma^L_{Q\pi\pi}=\Gamma^{\rm tree}_{Q\pi\pi}\times F^L_{Q\pi\pi}$, and $\Gamma^L_{Q\pi\pi}$ is the two-point proper function on the lattice, with one insertion of $Q^L(x)$, and calculated in the limit $a\to0$. The functions $Z^{\rm MS}_\pi(T,\mu,a)$ and $Z^{\rm MS}_t(T,\mu,a)$ are, respectively, the field and coupling renormalization constants that allow us to get, starting from the lattice regularization, the same Green's functions as those of the $\overline{\rm MS}$ renormalization scheme. In particular, $Z(T)$ can be obtained by imposing Eq. (23) at $p+q=0$.

FIG. 1. Diagrams contributing at one loop to the two-point proper function with one insertion of $Q(x)$. White blobs, black blobs, and black squares indicate, respectively, the operator vertices, the Lagrangian vertices, and the vertices coming from the measure term.

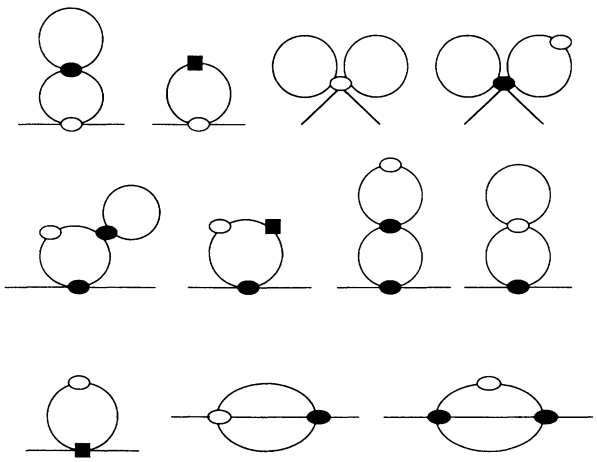

FIG. 2. Diagrams contributing at two loops to the two-point proper function with one insertion of $Q(x)$.

In order to calculate $Z(T)$ at two loops, we need to know $Z^{\rm MS}_\pi(T,\mu,a)$ to two loops and $Z^{\rm MS}_t(T,\mu,a)$ to one loop; they have been calculated in Ref. [24]:

$$Z^{\overline{\rm MS}}_\pi(T,\mu,a)=1-2L(a^2\mu^2)T+\{[L(a^2\mu^2)]^2-2c_1L(a^2\mu^2)+b_2\}T^2+O(T^3)\ ,$$
$$Z^{\overline{\rm MS}}_t(T,\mu,a)=1-[L(a^2\mu^2)+c_1]T+O(T^2)\ , \quad (24)$$

where $L(x)=-(1/4\pi)\ln x+(5/4\pi)\ln2-y$, the values of the numerical constants being $y=0.0472$, $b_2=-0.0116$, and $c_1=0.1703$.

We have calculated $F^L_{Q\pi\pi}$ at $p+q=0$ and at two loops. The diagrams at one loop and at two loops contributing to $F^L_{Q\pi\pi}$ are shown, respectively, in Figs. 1 and 2. We have found

$$F^L_{Q\pi\pi}(T,h,a;p,q)|_{p+q=0}=1+[2L(a^2h)+d_1]T+\{2[L(a^2h)]^2+2(c_1+d_1)L(a^2h)+d_2\}T^2+O(T^3)\ , \quad (25)$$

with $d_1=-0.6839$ and $d_2=-0.0753$.

Then by gathering the results in Eqs. (18) and (23)–(25), we finally get

$$Z(T)=1+z_1T+z_2T^2+O(T^3)\ ,$$
$$z_1=d_1\ , \quad (26)$$
$$z_2=d_2+b_2+\frac{c_1}{2\pi}\ .$$

That is, $z_1=-0.6839$ and $z_2=-0.0598$.

C. Contact terms

As stated in the Introduction, the other source of difficulties is the presence of contact terms in the operator-product expansion of $Q^L(x)Q^L(0)$ when $x \to 0$, which contribute to χ^L in the definition (6). They appear as mixings with the unity operator (the so-called perturbative tail) and the action density, $S(x)=[\partial_\mu \phi(x)]^2$, which are the only available O(3) invariant operators with dimension equal to or lower than 2. Then the theory of local operators leads to the relation (9) between χ^L and the physical χ. In Eq. (9) the quantity $\langle S(x) \rangle$ is intended to be the nonperturbative part of the expectation value of the action density; i.e., it is a signal of dimension d.

As $Z(T)$, $A(T)$, and $P(T)$ can be calculated in perturbation theory following the field-theory prescriptions. With our symmetrized definition of $Q^L(x)$, $P(T)$ starts from a T^4 term (corresponding to three-loop graphs), while $A(T)$ starts from a T^3 term (corresponding to two-loop graphs).

We calculated the perturbative tail $P(T)=\sum_{n=4} p_n T^n$ up to four loops. In Figs. 3 and 4 we show the diagrams at three and four loops, respectively. The results for infinite volume were

$$p_4=6.832\times 10^{-5}, \quad p_5=5.722\times 10^{-5} . \tag{27}$$

These numbers were extracted by performing numerical integrations at finite volume and extrapolating the results to infinite volume.

In the following we will neglect the mixing with the action density, whose first contribution comes at two loops from the graph drawn in Fig. 5 and it is O (β^{-3}). This is consistent (in a perturbative sense) with $Z(T)$ calculated up to two loops. Notice that $Z(T)$, $P(T)$, and $A(T)$ depend on the choice of the regularized version of $Q(x)$ and on the action, that is they are cutoff-dependent quantities.

III. NUMERICAL RESULTS

A. The Monte Carlo algorithm

The advantage of the tree-improved action with respect to the standard action is that the correlation length is much smaller in the expected scaling region [27]. This allows us to perform our simulations without them being too sensitive to critical slowing down. For this reason we have preferred to use a local procedure of updating (suitable for complete vectorization on parallel computers), even though for this model an efficient cluster algorithm is available [28]. Our Monte Carlo upgrading procedure was an adaptation for the O(3) σ model of the over-heat-bath proposed in Ref. [29] for SU(N) non-Abelian gauge theories.

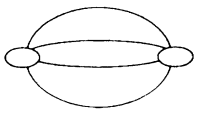

FIG. 3. Diagram contributing at three loops to the mixing with the unity operator.

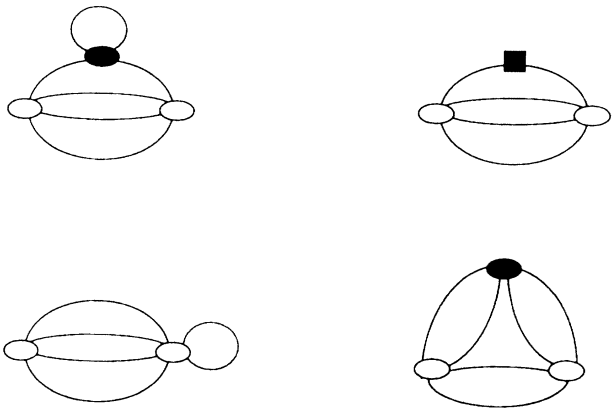

FIG. 4. Diagrams contributing at four loops to the mixing with the unity operator.

In the action S^L, the sum of the terms containing a given spin variable $\phi(x)$ can be written as the scalar product of two vectors:

$$S^L=-\beta\phi(x)F(x)+\cdots , \tag{28}$$

where the ellipsis indicates terms independent of $\phi(x)$. Therefore, only the angle ϑ between $\phi(x)$ and $F(x)$ enters S^L. By taking a frame where $F(x)$ is along the third direction, we extract the new variable ϑ with the distribution

$$dp(\cos\vartheta)=\exp(\beta|F|\cos\vartheta)d(\cos\vartheta) . \tag{29}$$

In a standard heat bath, the other angle φ is taken with a flat distribution. Instead, the over-heat bath chooses the new φ with the condition of minimizing the scalar product between the vector corresponding to the new spin variable and that of the old one. This condition consists in taking $\varphi_{\text{new}}=\pi+\varphi_{\text{old}}$. The detailed balance is satisfied because the additional condition is symmetric between the old and new links and drops in the ratio of direct and inverse transition probabilities. The over-heat-bath algorithm incorporates the requirements of a canonical energy distribution and of overrelaxation.

An alternative realization of overrelaxed algorithms consists in alternating microcanonical updatings with canonical ones (necessary to ensure the ergodicity of the algorithm). A microcanonical updating consists in choosing the new variable with the same energy as the old one but lying in the group space as far as possible from it. In the O(3) σ model a microcanonical updating is obtained by taking

$$\phi_i^{\text{new}}=\frac{2\phi^{\text{old}}F}{|F|^2}F_i-\phi_i^{\text{old}} . \tag{30}$$

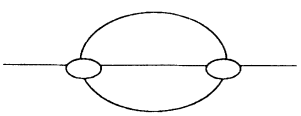

FIG. 5. Diagram contributing at two loops to the mixing with the action density. Its contribution is $O(\beta^{-3})$.

In the following we will consider an overrelaxed algorithm constructed by performing a sequence of nine microcanonical updatings and one over-heat-bath updating.

To test the performance of these algorithms, we calculated integrated autocorrelation times $\tau_{\rm int}^0$ of the normalized autocorrelation function $A_0(t)$ of two quantities: the energy E, and the magnetic susceptibility χ_m:

$$\tau_{\rm int}^0=\frac{1}{2}\sum_{t=-\infty}^{\infty}A_0(t)\ ,$$
$$A_0(t)=\frac{\sum_{n=1}^{N}[O(n+t)-\langle O\rangle][O(n)-\langle O\rangle]}{\sum_{n=1}^{N}[O(n)-\langle O\rangle]^2}\ , \tag{31}$$

where $O(n)$ is the average of the operator O on the nth configuration, N is the total number of sequential configurations, and the angular brackets indicate an average over the N configurations. For the overrelaxed algorithm, the time units are the single sweeps. To estimate $\tau_{\rm int}$ we employed a self-consistent truncation window of width $4\times\tau_{\rm int}$ [30]. The results are reported in Table I. The values of the correlation length ξ are obtained from the mass gap data reported in Ref. [27]. The values of β (and hence of ξ) and the size of the lattice L are chosen such that $L/\xi\simeq{\rm const}\simeq 3$.

As expected, the algorithms based on procedures of overrelaxation show a notable improvement with respect to the standard heat bath. Furthermore, taking a heat-bath iteration as a unit of computational time, the over-heat-bath and the overrelaxed algorithm take, respectively, the values $t\simeq 0.9$ and $\simeq 0.7$ per iteration.

Since χ_m is expected to couple strongly with the longest modes, we determine the dynamical critical exponent by identifying $\tau_{\rm int}\equiv\tau_{\rm int}^{\chi m}$. The parameter $\tau_{\rm int}$ is expected to behave asymptotically as $\tau_{\rm int}\simeq c\xi^z$, where c and z are constants that depend on the algorithm employed; z is the dynamical critical exponent. According to the finite-size scaling theory, c must be a function of the ratio ξ/L, $c\equiv f(\xi/L)$; therefore, keeping ξ/L constant, c behaves as a constant. In Fig. 6, a log-log plot of $\tau_{\rm int}$ versus ξ is shown. Data for the heat bath are compatible with $z_{\rm HB}\simeq 2$. By a best fit of the data we found, for the other two algorithms,

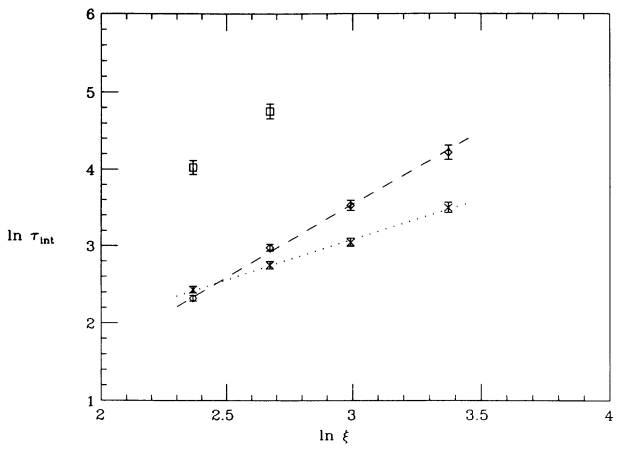

FIG. 6. Log-log plot of $\tau_{\rm int}^{\chi m}$ vs ξ for the heat-bath (square), the over-heat-bath (diamond), and the overrelaxes (cross) algorithms. The lines are the results of the fits.

$$z_{\rm OHB}=1.90\pm 0.08\ ,$$
$$c=0.11\pm 0.03\ , \tag{32}$$
$$\chi^2/N_{\rm DF}\simeq 0.8\ ,$$

for the over-heat bath, and

$$z_{9m+1{\rm OHB}}=1.03\pm 0.07\ ,$$
$$c=0.98\pm 0.20\ , \tag{33}$$
$$\chi^2/N_{\rm DF}\simeq 0.3\ ,$$

for the overrelaxed algorithm consisting of sequences of nine microcanonical sweeps and one over-heat-bath sweep. Although both algorithms contain overrelaxation procedures, their dynamic behavior is very different. On the other hand, it is well known that only an optimized overrelaxation can give $z\simeq 1$, which represents the free-field limit investigated by Adler [31]. Of course, to reach the equilibrium condition at a given β, the over-heat bath is the best algorithm in that it assures a canonical distribution.

TABLE I. $\tau_{\rm int}^E$ and $\tau_{\rm int}^{\chi m}$ versus β, the correlation length ξ, the size of the lattice L. HB, OHB, and 9m+1OHB indicate, respectively, heat-bath, over-heat-bath algorithm and the algorithm constructed by performing nine microcanonical iterations followed by an over-heat-bath sweep. Stat is the statistics used. Estimated errors in the least significant digits are shown in brackets.

β	ξ	L	MC	Stat	$\tau_{\rm int}^E$	$\tau_{\rm int}^{\chi m}$
1.32	10.64(7)	30	HB	100k	8.0(4)	56(5)
1.38	14.47(19)	45	HB	200k	8.3(3)	116(11)
1.32	10.64(7)	30	OHB	100k	2.2(1)	10.2(4)
1.38	14.47(19)	45	OHB	160k	2.5(1)	19.6(9)
1.44	19.92(24)	60	OHB	120k	2.4(1)	34.0(2.3)
1.50	29.15(42)	90	OHB	120k	2.0(1)	67.7(6.4)
1.32	10.64(7)	30	9m+1OHB	100k	13.5(8)	11.4(5)
1.38	14.47(19)	45	9m+1OHB	100k	12.6(7)	15.6(8)
1.44	19.92(24)	60	9m+1OHB	120k	12.6(7)	21.1(1.1)
1.50	29.15(42)	90	9m+1OHB	120k	11.4(6)	33.0(2.2)

Looking at Table I we see that the choice of the best algorithm depends on the quantity we want to measure (the over-heat bath is much more efficient in decorrelating such quantities as the energy) and on the values of the lattice size and the correlation length. To measure the local topological charge $Q^L(x)$ on lattices up to 90^2, we found more convenient to employ the over-heat-bath upgrading procedure. Of course, going to bigger and bigger lattices and correlation lengths, the algorithm with $z \simeq 1$ will become more and more convenient.

B. Results

To begin with, we performed runs on a 60^2 lattice to collect data over an extended range of β. About 30 values of β were chosen and about 40 000 sweeps were performed per value of β on the average. We used different binnings to safeguard our results from statistical correlation. Data for χ^L are reported in Table II.

The field-theoretical method consists in fitting expression (9) to Monte Carlo data in order to extract χ. A series of alternative fits can be performed on the data. Consistency requires that our results be stable under these variations. The mixing with unity operator constitutes a perturbative background to the Monte Carlo signal, and one must take good care to subtract it properly. While the first calculated terms of the perturbative tail, given in Eq. (27), fit the data extremely well at large β, more terms must be included as the scaling region is approached. Lacking an analytical calculation for the coefficients of these terms, one must fit them from the data. To estimate them, we fit data for $\beta \geq \beta^T = 1.8$, where the whole nonperturbative signal has exponentially died off. There, a total of four terms of the tail proves to be sufficient for a fit with $\chi^2/N_{\rm DF} \sim 1$. The coefficients fitted from data are $p_6 = -(6.9 \pm 0.4) \times 10^{-5}$ and $p_7 = (4.8 \pm 0.1) \times 10^{-4}$. Then we extrapolate and subtract $P(\beta)$ from all data. In Fig. 7 we plot

$$\frac{\chi}{\Lambda_{SY}^2} \equiv \frac{\chi^L(\beta) - P(\beta)}{Z(\beta)^2 f(\beta)^2} \tag{34}$$

in the presumed region of scaling. We see that the scaling is quite good. Fitting data with $\beta > \beta_{\rm min} = 1.4$ we obtain $\chi/\Lambda_{SY}^2 = (1.57 \pm 0.04) \times 10^2$ (with $\chi^2/N_{\rm DF} \simeq 0.4$). In the fit we have also taken into account the three-loop term in the scaling function of Eq. (16). A more reliable error is found by checking the stability of the result under various alternative fits: (a) different initial fits on the perturbative tail, (b) different values of β^T and $\beta_{\rm min}$, (c) global fits through the whole range of β including simultaneously the exponential and the tail parts. We have performed a systematic scan of such fits and concluded that the real uncertainty is about 10%.

We have performed a second set of simulations on a 90^2 lattice to check the importance of finite-size effects. Six values of β were chosen in the scaling region and 100 000 sweeps were performed per value of β. The results are reported in Table III. Since the mixing with the unity operator is a short-distance effect, we expect that the function $P(\beta)$ derived on the 60^2 lattice is still a good approximation of the perturbative tail. Then we subtract it from Monte Carlo data of the 90^2 lattice. In Fig. 8 we plot χ/Λ_{SY}^2 given by Eq. (34). The scaling is good and a fit (without the first data in Fig. 8) gives

TABLE II. χ^L and $\chi_{\rm cool}$ versus β on the lattice 60^2.

β	$10^5\chi^L$	$10^4\chi_{\rm cool}$
1.38	13.83(34)	
1.4	12.38(19)	3.3(2)
1.41	12.08(28)	2.8(2)
1.42	11.51(20)	2.65(30)
1.43	10.91(26)	2.2(2)
1.44	10.10(17)	2.1(1)
1.45	9.57(24)	1.8(3)
1.46	9.21(21)	
1.47	8.46(20)	1.4(2)
1.48	7.84(19)	
1.5	7.03(15)	1.1(1)
1.52	6.24(15)	0.9(2)
1.55	5.14(14)	0.55(15)
1.6	4.09(10)	
1.75	1.918(63)	
1.8	1.617(54)	
1.85	1.360(33)	
1.9	1.150(28)	
1.95	0.984(36)	
2.0	0.868(21)	
2.05	0.729(17)	
2.1	0.700(15)	
2.2	0.522(11)	
2.3	0.4194(96)	
2.5	0.2810(67)	
2.8	0.1664(37)	
3.0	0.1195(19)	
3.5	0.0611(15)	
4.0	0.034 20(53)	
5.0	0.012 69(37)	
10.0	0.000 737(31)	

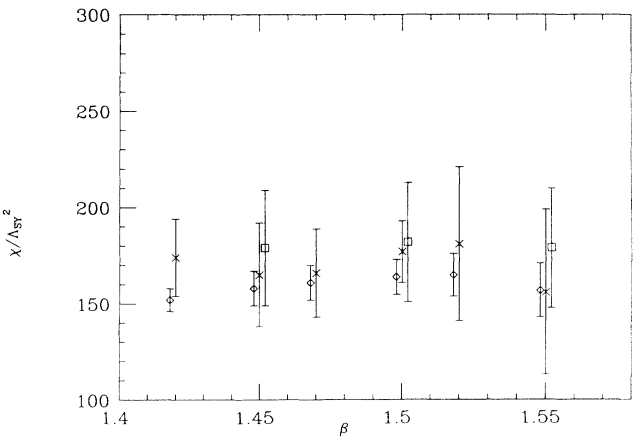

FIG. 7. Data from simulations on a 60^2 lattice: (a) $[\chi^L(\beta) - P(\beta)]/Z^2(\beta)_{2\ \rm loops} f^2(\beta)$ (diamond); (b) χ/Λ_{SY}^2 extracted by cooling (cross); (c) the same as in (a), but with $Z(\beta)$ determined by heating an instanton (square). For the sake of legibility, data (a) and (c) at the same value of β as (b) are slightly shifted in β.

TABLE III. χ^L and $\chi_{\rm cool}$ versus β on the lattice 90^2.

β	$10^5\chi^L$	$10^4\chi_{\rm cool}$
1.42	11.62(17)	3.1(3)
1.45	10.06(15)	2.1(2)
1.47	9.12(19)	1.65(15)
1.5	7.73(11)	1.36(16)
1.52	6.63(14)	1.07(17)
1.55	5.62(16)	0.70(9)

$\chi/\Lambda_{SY}^2=(1.9\pm0.1)\times10^2$ ($\chi^2/N_{\rm DF}\simeq0.5$), which is about 20% higher than the value found on the 60^2 lattice.

C. Cooling method

An independent method of χ can be obtained by the cooling technique [10], which consists in measuring the topological charge on an ensemble of configurations cooled by locally minimizing the action. This method relies on the assumption that local changes do not modify the topology of the configuration. By the cooling process, each configuration is transformed into a minimum of the action, i.e., into a classical configuration with the same topological charge. Local fluctuations are eliminated and Q can be read on the classical configuration.

Along with thermalization sweeps, we employed a cooling algorithm; its building block (a cooling step) is the assignment, to each spin variable ϕ, of a new value ϕ' which minimizes the action (keeping all other links fixed), subject to the constraint $(\phi-\phi')^2\le\delta^2$ [11]. The parameter δ limits the distance between the old and new values of the spin variable. We chose $\delta=0.1$ for our simulations. A cooling descent was performed typically every 200–500 thermalization sweeps depending also on β. Each cooling descent consisted of 30 steps, and averages were taken at each cooling step across all descents. We used the operator $Q^L(x)$ to determine the topological charge of the cooled configurations. We constructed ensembles of 100–400 configurations on the average per value of β and per cooling step. The topological susceptibility measured on cooled configurations by Eq. (6), $\chi^L_{\rm cool}$, is seen to gradually rise up to a very extended plateau, lasting beyond the 30 sweeps performed, until metastable structures carrying topological charge disappear. Our data along with their error are taken on the plateau; they are reported in Tables II and III. In Figs. 7 and 8 we plot data divided by $f^2(\beta)$ for the 60^2 and 90^2 lattices, respectively. A good scaling is observed for $\beta\ge1.4$. Fitting these data we obtain, respectively,

$$\frac{\chi}{\Lambda_{SY}^2}=(1.70\pm0.05)\times10^2\ ,$$
$$\frac{\chi}{\Lambda_{SY}^2}=(2.0\pm0.1)\times10^2\ , \tag{35}$$

in agreement with the determinations of χ by the field-theoretical method.

We have also followed the behavior of χ^L during cooling. As in Ref. [11], we introduce an effective temperature $\beta_{\rm eff}$ of the short-ranged fluctuations and we parametrize $\chi^L_{\rm cool}$ by the equation

$$\chi^L_{\rm cool}=Z(\beta_{\rm eff})^2a^2\chi+P(\beta_{\rm eff}) \tag{36}$$

(here we have left out the mixing with the action density), $\beta_{\rm eff}$ must be a function of the cooling step: at cooling step zero it equals β, while at the end of cooling $\beta_{\rm eff}\to\infty$, so that

$$Z(\beta_{\rm eff})_{\beta_{\rm eff}\to\infty}\to1,\quad P(\beta_{\rm eff})_{\beta_{\rm eff}\to\infty}\to0\ , \tag{37}$$

and therefore $\chi^L\to a^2\chi$, which explains the agreement of the determinations of χ by the field-theoretical method and the cooling method. A natural choice for $\beta_{\rm eff}$ is the one satisfying [11]

$$S_N=\langle S\rangle(\beta_{\rm eff})\sim\frac{1}{\beta_{\rm eff}}+\frac{0.0978}{\beta_{\rm eff}^2}\ , \tag{38}$$

where S_N is the average action on the sample $\{C_N\}$ constructed by performing N cooling sweeps starting from the configurations thermalized at a given β; the expression $\langle S\rangle(\beta)$ is the energy in statistical equilibrium at a given β. In Eq. (38) we have considered only the first two terms of the weak-coupling expansion of $\langle S\rangle(\beta)$. Of course, we are not in statistical equilibrium, and therefore $\beta_{\rm eff}$ is only an approximate concept, but, as we will see, in this off-equilibrium condition, it will give a good parametrization of the contributions of the fluctuations about the smooth background fields, which give origin to the physical topological susceptibility. According to Eq. (36) the expression

$$\{[\chi^L_{\rm cool}-P(\beta_{\rm eff})]/\chi a^2\}^{1/2} \tag{39}$$

as a function of cooling step (and hence of $\beta_{\rm eff}$) should coincide with the calculated $Z(\beta_{\rm eff})$. In Fig. 9 we compare the quantity (39) as a function of $\beta_{\rm eff}$ with the curve $Z(\beta_{\rm eff})_{2\,\rm loops}$ for data at $\beta=1.44$. The agreement of $Z(\beta_{\rm eff})_{2\,\rm loops}$ with data is satisfactory. Furthermore, this agreement allows us to use as a criterion for checking on eventual losses of topological charge during cooling [11], the way in which the cooling data follow the renormalization curve.

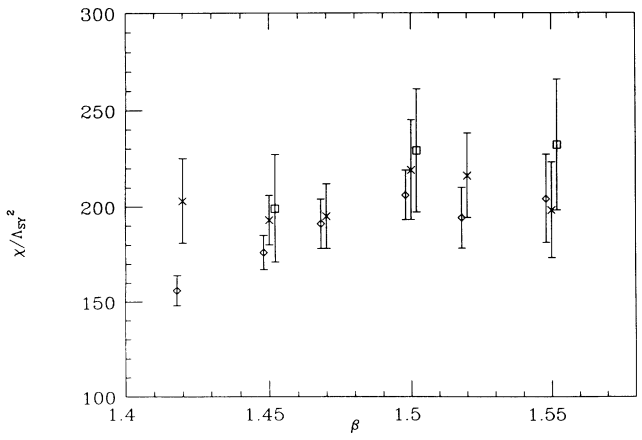

FIG. 8. The same as in Fig. 7 on a 90^2 lattice.

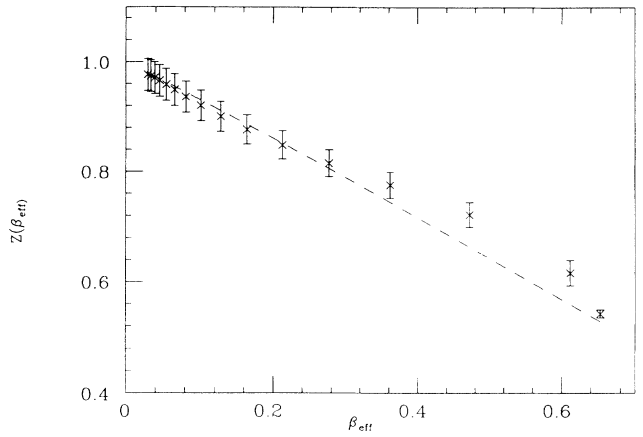

FIG. 9. The quantity in Eq. (39) is plotted vs cooling steps. For each cooling step we collected 750 configurations. We performed a cooling descent every 400 iterations, running at $\beta=1.44$ on a lattice 60^2. The dashed line is the curve $Z(\beta_{\rm eff})_{2\ \rm loops}$.

IV. NONPERTURBATIVE DETERMINATION OF THE RENORMALIZATIONS

A. The method

The fundamental point is that $Z(\beta)$, $P(\beta)$, and $A(\beta)$ have their origin in the short-ranged fluctuations ($l\sim a$), whereas the relevant topological properties are determined by fluctuations at a distance $l\sim\xi$. As in Ref. [32] we assume that, on the configurations relevant to the functional integral, the lattice topological charge can be expressed as

$$q^L(x)\simeq[Z(\beta)+\zeta(x)]q(x)+\eta(x)\ , \tag{40}$$

where $q(x)$ is a background topological charge density determined by the fluctuation at $l\sim\xi$, where ζ and η are random variables with zero averages ($\langle\zeta\rangle=\langle\eta\rangle=0$) and are determined by the short-ranged fluctuations. Relation (40) is an effective way of characterizing the different contributions to $\langle Q\rangle$ and $\langle Q^2\rangle$. It will receive further support from the consistency of the results. Approaching the continuum limit, ζ and η are expected to be independent of the background topological structure; they should decouple from $q(x)$, i.e., $\langle\zeta q\rangle=\langle\eta q\rangle=0$. According to the parametrization (40), the topological charge of a configuration is $Q=\sum_x q(x)$ and the topological susceptibility $\chi=\langle Q^2\rangle/V$. Instead, χ^L should be given by

$$\chi^L\simeq Z^2a^2\chi+\frac{\langle[\sum_x\eta(x)]^2\rangle}{V}+\frac{\langle[\sum_x\zeta(x)q(x)]^2\rangle}{V}\ . \tag{41}$$

Since the second term in Eq. (41) gives contributions of dimension zero, we can identify it with a mixing with the unity operator, while the third one should be related to the mixing with the action density.

If we are able to perform simulations keeping the background topological charge Q_0 fixed, Eq. (40) should give

$$\begin{aligned}&\langle Q^L\rangle|_{Q_0}\simeq Z(\beta)Q_0\ ,\\ &\chi^L|_{Q_0}\simeq\frac{Z(\beta)^2Q_0^2}{V}+\frac{\langle[\sum_x\eta(x)]^2\rangle}{V}\Big|_{Q_0}\\ &\qquad+\frac{\langle[\sum_x\zeta q]^2\rangle}{V}\Big|_{Q_0}\ ;\end{aligned} \tag{42}$$

$\langle[\sum_x\eta(x)]^2\rangle|_{Q_0}$ is expected to be independent of the background topological structure and therefore its contribution should be the same as that of the corresponding term in Eq. (41).

To perform the measurements suggested by Eq. (42), we employ a method inspired by Ref. [32]. We start from a given large classical configuration C_0, having topological charge Q_0, and construct ensembles of configurations $\{C_n\}$ obtained by performing n local Monte Carlo sweeps, at a given β, starting from C_0. For small n, we expect that the long-distance properties, and in particular the topological charge, of the configurations belonging to $\{C_n\}$ will be the same as those of C_0, and that only the short-distance fluctuations will vary among $\{C_n\}$. Of course, how big we can take n without losing the memory of C_0 depends on the upgrading procedure. We expect that, if $\xi\gg a$, there exists an intermediate range of n where fluctuations of length $l\sim a$ are thermalized at the given value of β and give the renormalization effects, but where those at $l\sim\xi$ are off equilibrium and are still determined by the initial configuration. Measuring $Q^L(x)$ on the ensembles $\{C_n\}$, we should find $\langle\sum_x Q^L(x)\rangle_n\simeq Z(\beta)Q_0$ for n big enough to have thermalized fluctuations at $l\sim a$ and small enough to have left intact the structure at $l\sim\xi$. Furthermore, if the renormalization functions are really caused by fluctuations at $l\sim a$, we do not expect to observe the effects of critical slowing down on their measurement. This should instead affect the length of the intermediate range of n where the above phenomenon can be observed: at that point, the Monte Carlo is going to change the physical modes that determine the topological properties. To be sure that during the heating we are not changing the background topological structure of the initial configuration, after $\bar n$ heating sweeps we cool the configurations (minimizing the action locally) and check, on cooled configurations, that the topological charge still has value Q_0.

As an updating procedure we use the standard heat bath, which gives a mild heating. To our purpose, the over-heat-bath algorithm loses the memory of the initial configuration too rapidly.

B. Nonperturbative determination of $Z(\beta)$

To begin with, we determine $Z(\beta)$ by heating an instanton configuration. We construct a discretized instanton by setting

$$\frac{\phi_1(x)+i\phi_2(x)}{1+\phi_3(x)}=\frac{z-r}{z-s}\ , \tag{43}$$

where $z=x_1+ix_2$, r and s being two complex numbers. We have taken $r=L/3-0.5+iL/2$ and

$s=2L/3+0.5+iL/2$, where L is the size of the lattice. Furthermore, we perform a few cooling steps to make the configuration smoother. After this procedure, we end up with a configuration C_0 with topological charge $Q_0 \simeq 1$. In Fig. 10 we plot Q_n/Q_0, where Q_n is the topological charge averaged on the ensemble $\{C_n\}$. Data are taken on a 120^2 lattice. Each ensemble contains 1000 configurations. From 1 to $\bar{n}=15$ we thermalize at $\beta=1.55$, then we cool the configurations. We see clearly a plateau from $n \sim 5$ until cooling starts. After a few steps, the cooling process gives $Q \sim Q_0$, showing that the background structure remained unchanged during the thermalization.

According to Eq. (42), the value of $\langle Q^L \rangle$ at the plateau gives an estimate of $Z(\beta)$. Averaging data in the plateau (that is from $n=6$ to $n=15$), we obtain $Z(1.55)=0.50\pm0.02$ (as error we take the typical error of data in the plateau) to be compared with the two-loop result [Eq. (26)] $Z(1.55)_{2\,\text{loops}}=0.534$. We have repeated all this at different values of β, on different lattices, and for different values of Q_0. As in Fig. 10, we see in all cases a very clear plateau. In Table IV we give the results and their comparison with the two-loop approximation of $Z(\beta)$. The values of $Z(\beta)$ are systematically lower than $Z(\beta)_{2\,\text{loops}}$, typically by about 5% in the scaling region. In Figs. 7 and 8 the ratio χ/Λ_{SY}^2 corrected by using the measured value of $Z(\beta)$ in Eq. (34) is also shown.

Notice that plateaus always start from $n \sim 5$, proving that the quantity $Z(\beta)$ is not subject to critical slowing down. This confirms that fluctuations contributing to $Z(\beta)$ are those at $l \sim a$. On the other hand, by increasing β or the size of the initial instanton, plateaus become longer.

By using the same procedure, we have also observed what happens when measuring the topological charge by the geometrical method [13]. Starting from an instanton configuration, if it were a reliable measure of Q, we would expect to find always $Q=1$, since we are sure that during the process the underlying topological structure is not changed. Instead, several times we found $Q \neq 1$ (although still an integer) after a few sweeps of heating even for values of β corresponding to very large ξ. This shows how this definition of Q is sensitive to an unphysical contribution coming from fluctuations of length $l \sim a$, and therefore that it is not good for measuring χ.

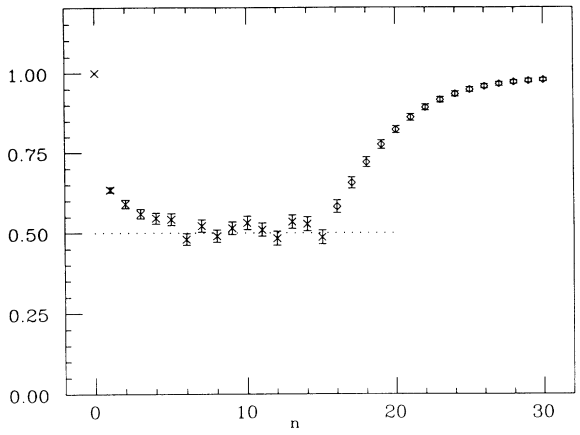

FIG. 10. Q_n/Q_0 vs n. Data with the cross symbol refer to the thermalization process, while data with the diamond symbol refer to the cooling procedure. The thermalization is performed by a heat-bath algorithm at $\beta=1.55$ on a 120^2 lattice. The dotted line indicates the value of $Z(\beta)$ estimated by averaging data at the plateau.

As an example of the performance of the over-heat-bath algorithm in this context, we mention that on a 60^2 lattice, starting from an instanton configuration and heating at $\beta=1.6$, it takes ~ 5 sweeps to bring the average topological charge to zero.

C. Nonperturbative determination of the mixing with the unity operator

By using the same procedure, we now measure χ^L. If the starting configuration C_0 is constructed by setting $\phi(x)=(1,0,0)$, according to Eq. (42) we should get a direct estimate of the perturbative tail. Starting from C_0, we thermalize at various values of β on a 60^2 lattice, col-

TABLE IV. $Z(\beta)$ versus β. L is the size of the lattice, Q_0 is the topological charge of C_0, N_{conf} is the number of configurations of each ensemble $\{C_n\}$. The fourth column indicates the heating sweeps at which the plateau is observed. The error on $Z(\beta)$ is the typical error of data in the plateau. The last column gives the perturbative renormalization function calculated at two loops.

β	L	Q_0	N_{conf}	Plateau	$Z(\beta)$	$Z(\beta)_{2\,\text{loops}}$
2.0	60	0.990	400	6–15	0.635(10)	0.643
2.0	120	0.997	400	6–15	0.63(2)	0.643
1.8	60	0.990	400	6–15	0.58(1)	0.602
1.7	60	0.990	400	6–15	0.55(1)	0.577
1.6	60	0.990	1000	6–10	0.52(1)	0.549
1.6	120	0.997	1000	6–15	0.53(2)	0.549
1.6	120	1.982	1000	6–10	0.52(1)	0.549
1.6	120	3.960	1000	6–10	0.51(1)	0.549
1.55	60	0.990	1000	6–10	0.50(1)	0.534
1.55	120	0.997	1000	6–15	0.50(2)	0.534
1.5	60	0.990	1000	6–8	0.48(2)	0.517
1.5	120	0.997	1000	6–10	0.49(2)	0.517
1.45	120	0.997	1000	6–10	0.47(2)	0.500

lecting 1000 configurations per ensemble $\{C_n\}$. In Fig. 11 we show data at $\beta=2$, i.e., where the expected nonperturbative signal is much smaller than the perturbative tail. We see that around $n\sim 20$, the data reach the value obtained by a standard Monte Carlo simulation in the equilibrium condition. In Fig. 12 we show data at $\beta=1.6$. Again starting from $n\sim 20$, a plateau is observed, but this time at a lower value than when χ^L was measured by the standard Monte Carlo simulation (see Table II). After a long plateau, the data go up to reach the equilibrium value of χ^L. In the middle of the plateau, after 40 sweeps we started to cool configurations to check that topological charge was not created during the heating; indeed, χ^L goes to zero during cooling. Data at $\beta=1.5$ are plotted in Fig. 13. We again see a plateau starting from $n\sim 20$, but lasting less than that at $\beta=1.6$.

We identify the quantity measured by the position of the plateau χ_p^L with the perturbative tail at a given value of β. This interpretation is supported by the following observations.

(i) The starting point of the plateaus does not change by varying β. It means that the quantity measured by those plateaus, χ_p^L, is not sensitive to critical slowing down. Since we are using a local algorithm, this shows that χ_p^L is generated by fluctuations at $l\sim a$, as the mixing with the unity operator is supposed to be. Repeating the procedure on the 30^2 lattice, we have found the same results for χ_p^L, without observing finite-size effects.

(ii) The length of the plateaus, l_p, increases with β. The increase of l_p as a function of β is compatible with $l_p\sim\xi^\alpha$ and with $\alpha\sim 2$. We recall that the dynamical exponent z of the heat-bath algorithm is $z\simeq 2$, and therefore physical fluctuations at $l\sim\xi$ are expected to reach the statistical equilibrium with a time $\tau\sim\xi^2$.

Remarks (i) and (ii) are confirmed by the data at $\beta=1.45$ and 1.55. As a best estimate of χ_p^L, we take the average of the data in the observed plateau, and as error the typical error of data in the plateau. In Table V we report the values of χ_p^L versus β; we compare them with the estimate of $P(\beta)$ by perturbation theory given in Sec. II C, finding good agreement.

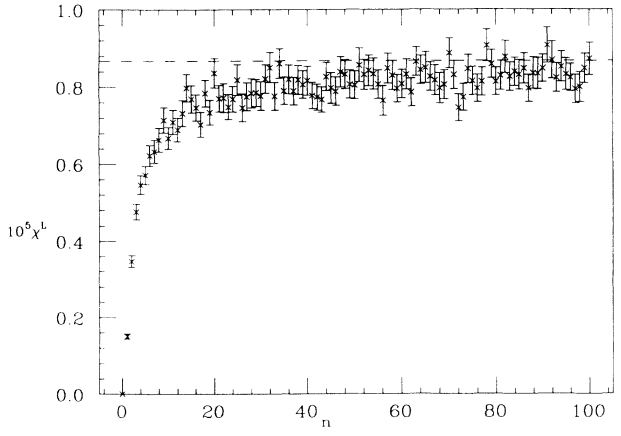

FIG. 11. χ^L vs n. Data are taken starting from a flat configuration and heating at $\beta=2$ on a 60^2 lattice. The dashed line is placed at the value obtained by a standard Monte Carlo simulation: $\chi^L=(8.68\pm 0.21)\times 10^{-6}$.

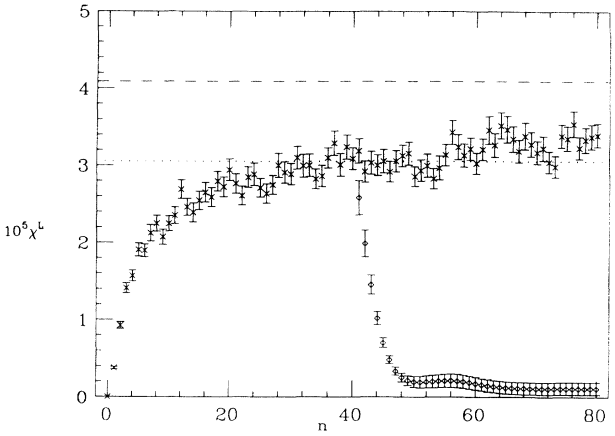

FIG. 12. χ^L vs n at $\beta=1.6$, starting from a flat configuration on a 60^2 lattice. Data with cross symbol refer to the thermalization process, while data with diamond symbol to the cooling procedure. The dashed line gives χ^L measured by a standard Monte Carlo simulation. The dotted one indicates the value of χ_p^L estimated by averaging data at the plateau (see Table V).

We also measure χ^L starting from an instanton configuration. We define the quantity δ as

$$\delta=\chi^L-\chi_p^L-Z(\beta)^2Q_0^2/V\ , \tag{44}$$

with $\chi_p^L=\langle[\sum_x\eta(x)]^2\rangle_n/V$ obtained starting from the flat configuration (see Table V); δ should measure the third term in Eq. (42). In Fig. 14 we plot δ versus n at $\beta=1.55$ and 1.6. We observe a clear plateau whose position is compatible with zero. The above behavior is also observed when starting from configurations with $Q_0\simeq 2$ and $\simeq 4$. This shows that the third term in Eq. (42) gives small contributions, confirming the perturbative result for which $A(\beta)$ starts only from a β^{-3} term. Moreover, it confirms that $\chi_p^L=\langle[\sum_x\eta(x)]^2\rangle_n/V$ is independent of the background topological structure.

To conclude, we have seen that the mixing with the unity operator is a well-defined quantity and we have obtained a direct reliable estimate of it. The success of the

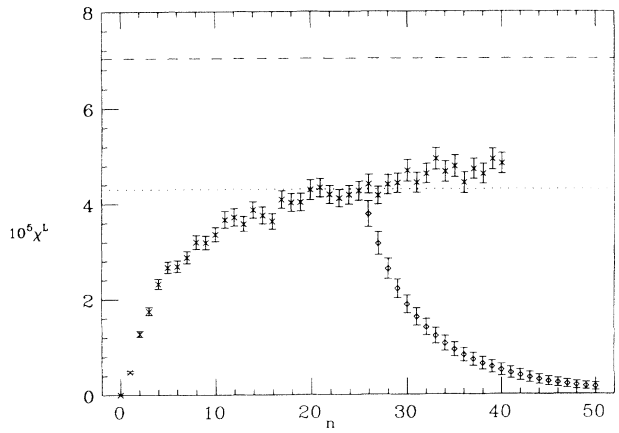

FIG. 13. The same as in Fig. 12, at $\beta=1.5$.

TABLE V. χ_P^L versus β. χ_P^L is determined averaging data in the observed plateau. The error on χ_P^L is the typical error of data in the plateau. L is the size of the lattice, each ensemble $\{C_n\}$ contains 1000 configurations. $P(\beta)_{\text{pert}}$ is the estimate of the perturbative tail by perturbation theory given in Sec. III B. χ^l is the value obtained by a standard Monte Carlo simulation on a 60^2 lattice.

β	L	$10^5\chi_P^L$	$10^5 P(\beta)_{\text{pert}}$	$10^5\chi^L$
1.6	30	3.10(15)	2.97(6)	
1.6	60	3.05(10)	2.97(6)	4.09(10)
1.55	60	3.55(15)	3.56(8)	5.14(14)
1.5	30	4.25(25)	4.31(10)	
1.5	60	4.30(20)	4.31(10)	7.03(15)
1.45	60	5.35(25)	5.27(12)	9.57(24)

numerical method employed relies on the distinction between the fluctuations at distance $l \sim a$, contributing to the renormalizations, and those at $l \sim \xi$ determining the relevant topological properties. We have seen that fluctuations at $l \sim a$ are soon thermalized, whereas the topological charge thermalization is much slower, allowing a direct determination of both multiplicative and additive renormalizations. These results give further insight into the origin of the renormalization effects.

V. CONCLUSIONS

We have shown in this paper that the topological susceptibility can be extracted from lattice simulations by conventional methods of quantum field theory. We have estimated by perturbation theory the renormalization functions entering the relation between χ and the corresponding quantity measured on the lattice. We have used them to extract χ from a Monte Carlo simulation. An independent measure of χ has been obtained by cooling.

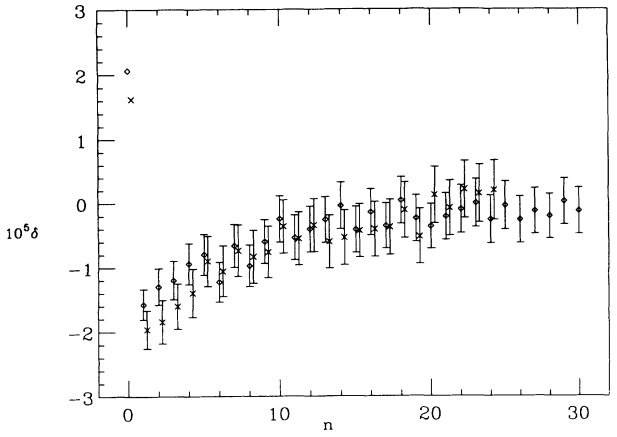

FIG. 14. δ vs n at $\beta=1.6$ (diamond) and at $\beta=1.55$ (cross, and slightly shifted in n) starting from an instanton configuration on a 120^2 lattice.

The two determinations are consistent with each other. Furthermore, we have given a direct estimate by Monte Carlo techniques of the additive and multiplicative renormalizations, finding good agreement with the estimates obtained by the perturbative approach. This shows, on the one hand, that the renormalization functions, both additive and multiplicative, are well-defined quantities, and, on the other hand, that they are well approximated, in the relevant range of the cutoff, by the perturbative approach.

ACKNOWLEDGMENTS

We wish to thank Massimo Campostrini, Giampiero Paffuti, Haris Panagopoulos, and Paolo Rossi for useful and stimulating conversations.

[1] G. 't Hooft, Phys. Rev. Lett. **37**, 8 (1976); Phys. Rev. D **14**, 3432 (1976).
[2] E. Witten, Nucl. Phys. **B156**, 269 (1979).
[3] G. Veneziano, Nucl. Phys. **B159**, 213 (1979).
[4] A. Di Giacomo, F. Farchioni, A. Papa, and E. Vicari, Phys. Lett. B **276**, 148 (1992).
[5] A. Di Giacomo and E. Vicari, Phys. Lett. B **275**, 429 (1992).
[6] A. D'Adda, M. Lüscher, and P. Di Vecchia, Nucl. Phys. **B146**, 63 (1978).
[7] R. J. Crewther, Nuovo Cimento **2**, 8 (1979).
[8] P. Di Vecchia, K. Fabricius, G. C. Rossi, and G. Veneziano, Nucl. Phys. B **B192**, 392 (1981); K. Ishikawa, G. Schierholz, H. Schneider, and M. Teper, Phys. Lett. **128B**, 309 (1983).
[9] M. Campostrini, A. Di Giacomo, and H. Panagopoulos, Phys. Lett. B **212**, 206 (1988).
[10] E. M. Ilgenfritz, M. L. Laursen, M. Müller-Preussker, G. Schierholz, and H. Shiller, Nucl. Phys. **B268**, 693 (1986); M. Teper, Phys. Lett. B **171**, 81 (1986); **171**, 86 (1986); J. Hoek, M. Teper, and J. Waterhouse, *ibid.* **180**, 112 (1986); Nucl. Phys. **B288**, 589 (1987).
[11] M. Campostrini, A. Di Giacomo, H. Panagopoulos, and E. Vicari, Nucl. Phys. **B329**, 683 (1990); in *Lattice, '89,* Proceedings of the International Symposium, Capri, Italy, 1989, edited by R. Petronzio *et al.* [Nucl. Phys. B (Proc. Suppl.) **17**, 634 (1990)].
[12] M. Campostrini, A. Di Giacomo, Y. Gündüç, M. P. Lombardo, H. Panagopoulos, and R. Tripiccione, Phys. Lett. B **252**, 436 (1990).
[13] B. Berg and M. Lüscher, Nucl. Phys. **B190**, 412 (1981).
[14] M. Lüscher, Commun. Math. Phys. **85**, 29 (1982).
[15] A. Phillips and D. Stone, Commun. Math. Phys. **103**, 599 (1986).
[16] P. Woit, Phys. Rev. Lett. **51**, 638 (1982); Nucl. Phys. **B262**, 284 (1985).
[17] M. Göcheler, A. S. Kronfeld, M. L. Schierholz, and U. J. Wiese, Nucl. Phys. **B292**, 330 (1987); A. S. Kronfeld, A. L. Laursen, G. Schierholz, and U. Wiese, *ibid.* **B292**, 330 (1987).
[18] M. Lüscher, Nucl. Phys. **B200**, 61 (1982).
[19] D. J. R. Pugh and M. Teper, Phys. Lett. B **218**, 326 (1989).
[20] A. Di Giacomo, in *QCD '90,* Proceedings of the International Workshop, Montpellier, France, 1990, edited by S.

Narison [Nucl. Phys. B (Proc. Suppl) **23A**, 191 (1991)].
[21] M. Campostrini and P. Rossi, Phys. Lett. B **272**, 305 (1991).
[22] M. Lüscher and D. Petcher, Nucl. Phys. **B225**, 53 (1983).
[23] K. Symanzik, Nucl. Phys. **B226**, 205 (1983).
[24] M. Falcioni and A. Treves, Nucl. Phys. **B265**, 671 (1986).
[25] E. Brezin and J. Zinn-Justin, Phys. Rev. D **14**, 3110 (1976).
[26] B. Allés and E. Vicari, Phys. Lett. B **268**, 241 (1991).
[27] P. Hasenfratz and F. Niedermayer, Nucl. Phys. **B337**, 233 (1990); in *Lattice '89* [11], p. 319.
[28] U. Wolff, Phys. Rev. Lett. **62**, 361 (1989).
[29] R. Petronzio and E. Vicari, Phys. Lett. B **254**, 444 (1991).
[30] N. Madras and A. D. Sokal, J. Stat. Phys. **50**, 109 (1988).
[31] S. Adler, Phys. Rev. D **37**, 458 (1988).
[32] M. Teper, Phys. Lett. B **232**, 227 (1989).